Compact MEMS-Based Fabry-Perot Interferometers for Space Applications

David Wolter^a, Matthias Grott^a, Jörg Knollenberg^a, Lynn Miller^a, Christian Althaus^a, Toni Großmann^b, Julia Wecker^b, Jörg Martin^b, Andreas Ihring^c, Boris Jung^a, Konstantinos Vasiliou^a, and Benjamin Fechtig^a

^aGerman Aerospace Center, Institute of Space Research, Berlin, Germany ^bFraunhofer Institute for Electronic Nano Systems, Chemnitz, Germany ^cLeibniz Institute of Photonic Technology, Jena, Germany

ABSTRACT

We present the design and first test results for a compact point spectrometer for space applications. The instrument operates in the thermal infrared wavelength range between 7.5 and 10.5 µm and uses thermopile detectors as a sensing element. Spectra are generated in the time domain by employing an electrically tunable MEMS-based Fabry-Perot filter. The overall mass of the instrument including electronics is around 300 g and the miniaturized design is suitable for use on small platforms like CubeSats or (micro)landers. The spectral resolution achieved by the instrument is around 30, sufficient to identify the broad spectral features typically present in rock forming minerals.

Keywords: Infrared, Fabry-Perot, Spectrometer, Space Exploration

1. INTRODUCTION

Due to the stringent constraints concerning the availability of engineering resources in terms of mass, volume, and power, the miniaturization of scientific instrumentation for planetary exploration missions has attracted significant attention. Scientific instruments for small platforms like CubeSats, microlanders or rovers need to comply with particularly stringent constraints concerning the available resources. Therefore, the use of highly integrated solutions for electrical and optical components has become increasingly common. Here we report on the development of a thermal-infrared point spectrometer for space applications, which is based on electrically tunable MEMS-based Fabry-Perot filters and thermopile detectors.

For the present instrument development, we target the thermal infrared wavelength range, as this is particularly suited to identify rock forming minerals^{1,2} through spectral features known as the Christiansen feature between 7.5 and 9 µm, as well as Reststrahlen bands and Transparency features between 10 and 13 µm. In addition, sulphates and phosphates show features between 8 and 10 µm. Apart from being relevant to decipher, e.g., the magmatic history of planetary bodies, many of these minerals are also potential feedstock for in-situ resource utilization processes³ like in-situ concrete production,^{4,5} oxygen production,^{6,7} or fibre production for additive manufacturing.⁸ As relevant spectral features are usually quite broad, moderate spectral resolutions of $\lambda/\Delta\lambda$ around 50 are largely sufficient for the characterization of rock-forming minerals and the identification of raw materials relevant for in-situ use.

The design of spectrometers can be based on various methods for generating the spectra, and a wide range of technical solutions can be implemented. For space applications, these range from interferometric approaches using Fourier transform spectrometers (FTIR)⁹⁻¹¹ to classical gratings,¹²⁻¹⁷ multi-spectral instruments using bandpass filters,^{18,19} and acoustically or electrically tunable optical filters.^{20,21} To obtain spatially resolved information, point spectrometers like Fourier transform spectrometers can use scan mirrors to resolve the scene, while grating spectrometers usually work in push-broom mode. On the other hand, acoustically tunable spectrometers obtain spatially resolved images directly while the spectrum is generated in the time domain by successively recording

Send correspondence to David Wolter, E-mail: david.wolter@dlr.de, Telephone: 0049 30 67055 331

monochromatic images at different wavelengths. For small satellites and landed platforms, compact Fourier transform spectrometers and spectrometers employing acoustically tunable filters are commonly used.

As ground smear is of no concern for landed platforms, instruments on the respective missions can generate spectra in the time domain without loss of scientific performance. So far, the use of acoustically tunable filters in solar system exploration has been limited to the wavelength range of $0.45-2.4 \,\mu\text{m}^{21}$ and $0.9-3.5 \,\text{m},^{20}$ although applications up to 5 μ m are being studied.²² One drawback of acoustically tunable filters is that they require relatively high power for control,^{20,23} which complicates their use in the thermal-infrared spectral range. Such limitations do not apply to Fabry-Perot filters based on MEMS technology.

For these filters, the pass-band can be tuned using electrostatic voltages and piezo-electrical actuation and the principle has been demonstrated over a large range of wavelengths. Electrically tunable Fabry-Perot filters have been designed for use in the visual wavelength range between 450 bis 550 nm, 24 854 nm, 25 and to 678 nm, 26 and filters have also been produced for operation in the mid-wave infrared. Further, dual-band FPIs which operate in the 3.1 µm to 3.7 µm and 4.0 µm to 4,6 µm wavelength range as well as in the 4 µm to 5 µm and 8 µm to 11 µm (LWIR) range have been developed. In general, the spectral resolution of these filters is around $\lambda/\Delta\lambda \approx 35$ to 75, and while most developments have been carried our for terrestrial applications, MEMS based Fabry-Perot spectrometers for use in space applications have been developed for the visual wavelength range.

The current filter design uses bulk micro-mechanical tunable Fabry-Perot filters originally developed for infrared gas analysis.³² The filter's optical cavity consists of two movable mirrors which form the optical resonator, whose optical length can be varied electrostatically. This approach helps to reduce the necessary control voltage and the filter has been designed to operate in the 7.5 µm to 10.5 µm wavelength range using Bragg reflectors. The chosen material system minimizes the internal stresses of the Bragg reflector layers and increase the optical throughput to over 80%. Further, it results in greater optical finesse, less warping, and better alignment of the reflectors to each other.³⁰ The filter is characterized by a small size of only 8.5 mm x 8.5 mm and thus fits the dimensions of typical TO (transistor outline) packages. Shock tests have shown the design to be robust up to 1500 g.³³

2. SPECTROMETER DESIGN

2.1 Optomechanical Design

The implemented spectrometer design is based on heritage from radiometers built for planetary exploration missions 14,19,34 and uses thermopile detectors 35 as a sensing element. Due to their broadband absorption and large area, such detectors are particularly suited for the current application and yield a large signal to noise ratio. At the same time, detectors do not need to be cooled, minimizing power uptake, size, weight, and complexity of the instrument. Electrically tunable micro-electromechanical Fabry-Perot filters 30 act as an additional optical element to generate the spectra in the time domain. We operate the filter in the first interference order and therefore the maximum free spectral range of the instrument is half the central wavelength. For the current application, the central wavelength was chosen to be 9 μ m with a usable wavelength range from 7.5 μ m to 10.5 μ m when applying a control voltage for tuning the central wavelength of the FPI between 0 and 70 V.

Thermopile sensors and Fabry-Perot filters have been integrated into standard transistor outline (TO) hermetic package with a diameter of 15 mm and a height of 5 mm. These are shown in light-red (thermopile) and cyan (FPI) in the cut views of the TO-package on the right hand side of Fig. 1. Furthermore, a PCB for electrical connections (green) as well as a spacing element (yellow) are integrated into the stack. Electrical connections are provided by bond-wires which connect thermopile and the PCB, which roots the lines to the TO-pins. These are in turn bonded to the PCB. For the FPI connections, these are directly bonded to the TO-package pins.

The instrument optics have been designed to satisfy the scientific measurement requirements of the Lunar Leaper Mission³⁶ and allow for a meter-scale ground sampling distance at a distance to target of around 50 m. This translates into an instantaneous field of view of 24.5 mrad. The optical tube assembly uses germanium plano-convex anti-reflection coated lenses with a diameter of 12.7 mm and a focal length of 20 mm, which are commercially available (yellow on the left hand side of Fig. 1). A germanium based order selection (bandpass) filter (dark red in Fig. 1) is used to block higher interference orders at short wavelengths and prevents leakage radiation from reaching the sensor at longer wavelengths. The sensor head has a diameter of 40 mm, a length of 45 mm, and a total mass of 105 g.

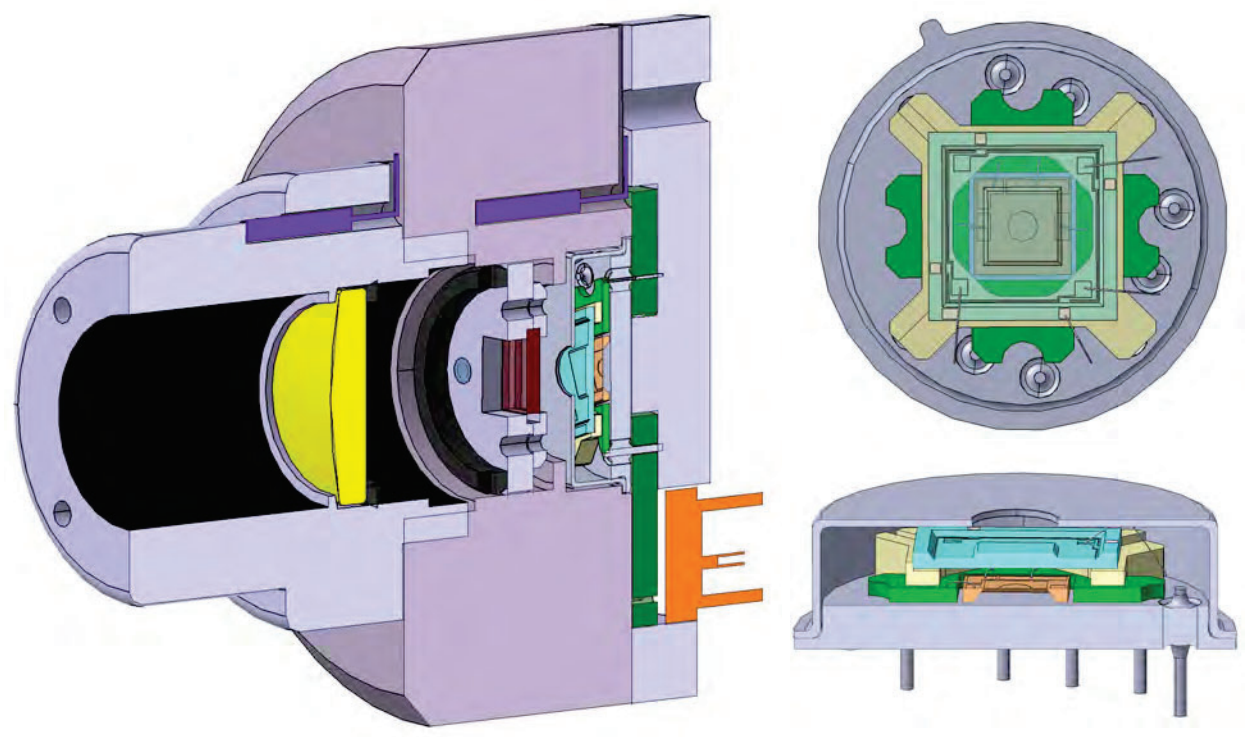


Figure 1: Left: Cut view of the spectrometer sensor head showing the baffle (black), lense (yellow), order blocking filter (red), FPI filter (cyan) and thermopile (orange). Top Right: Top view of the FPI sensor and filter assembly. Bottom Right: Cut view of the sensor including the Fabry-Perot filter (cyan) and thermopile sensor (orange).

2.2 Electrical Design

For the test results presented below, both the FPI as well as the thermopile detector have been operated using bench electronics. However, instrument electronics development based on a heritage read-out circuit³⁴ is currently ongoing. Functional sub-units of the electronics consist of a digital part for instrument commanding and control, an analogue part for thermopile signal conversion and house-keepings, a control voltage generation part to provide the 70 V needed to operate the FPI filter, as well as the sensor head which houses the thermopile, FPI filter, and PT1000 sensors. Electronics will be designed to fit two PC/104 printed circuit boards and the total mass of the boards is estimated to be 200 g if space grade components are to be used. A block diagram of the spectrometer electronics is shown in Fig. 2. If digital electronics for instrument commanding and control could be performed on the satellite or lander central control unit, the space and mass requirements of the Fabry-Perot spectrometer could be reduced to one PC/104 board and 100 g, respectively.

The digital control of the instrument will be implemented in a rad-tolerant flash FPGA of type ProAsic3 from Microsemi. The necessary 1.5 V core voltage and the 3.3 V will be generated from the spacecraft provided 5 V power rail using a line regulator. The FPGA controls all instrument functions in terms of the acquisition of samples from the science and house-keeping ADCs, the generation of the FPI control voltages, as well as the communication with the satellite's or rover's on-board computer. The acquisition of samples as well as the generation of spectra by stepping through the control voltage range will be implemented by operation modes. For commanding and data, an RS422 serial link will be implemented. As a baseline, no internal mass memory is foreseen and data will need to be regularly polled by the OBC for delivery and storage. If desired, a temperature control loop using a PID controller could be implemented in the FPGA, as was done for the Hayabusa2¹⁹ and InSight³⁴ missions.

The processing chain for the analogue signals consists of an input low-pass filter and signals are transferred differentially to a sigma/delta ADC of type ADS1258 with a resolution of 24 Bit. These ADC's incorporate an eight-channel differential multiplexer and have the additional advantage that optimal signal conditioning can

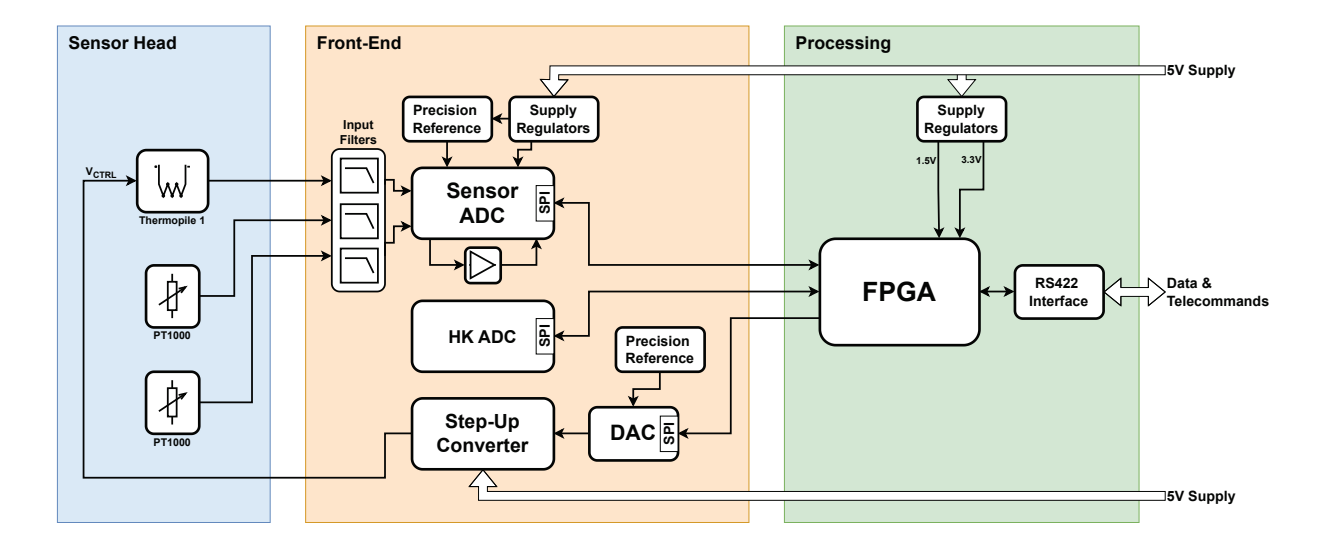


Figure 2: Block diagram of the spectrometer electronics consisting of the digital electronics, which interfaces with the satellite or lander, the analogue electronics, the control voltage generation, and the spectrometer sensor head housing thermopile, FPI, and PT1000 sensors.

be realized using an external, user defined circuit. Here, an external instrumentation amplifier topology with a gain of G=11 is used to provide the necessary high input impedance for the thermopiles with their source resistance of about 20 k Ω . Due to the placement of the external signal conditioning circuit between MUX output and ADC input, this amplifier can be incorporated into the internal self-calibration feature of the ADS1258, where electrical chopping of the signal is used to reduce offset voltage drifts to a minimum, a feature which is very important for the small signal voltages provided by thermopile detectors. Housekeeping measurements of voltages, currents, and temperatures will also be acquired using an ADS1258 ADC in addition to the one used to convert the thermopile signals.

The control voltage for the MEMS-based Fabry-Perot filter will be generated by a step-up converter circuit which operates from bus voltages as low as 5 V and which is capable of supplying an adjustable output voltage in the range of 0 V to slightly above 70 V. The control loop is built around the QMLV current-mode PWM-controller UC1843. To enable the large conversion factor of $V_{\rm Out}/V_{\rm In}=70~{\rm V/5~V}=14$, a Villard cascade has been integrated in the output filter circuit. The control voltage is created using a precision voltage reference and a simple SPI-controlled 12-Bit DAC of type DAC121S101. The minimum output voltage achievable by the circuit is 3.26 V and a control voltage of 0 V will be generated by switching the output to GND.

3. SPECTRAL CALIBRATION

Spectral calibration of the instrument has been performed at DLR's Detector Characterization Lab^{37,38} (DCL) using bench electronics. The setup consists of a cavity blackbody, an optical relay which provides an intermediate focus, a filter wheel located in the intermediate focus, an off-axis collimator, and a cryostat. Details of the optical layout of the setup are shown in Fig. 1 of the respective publication.³⁸ The setup in the DCL is shown in Fig. 3, where the cryostat and thermal vacuum cryostat are shown on the left hand side of the figure. A close-up of the cryostat, which houses the spectrometer, is shown in the middle panel of the figure, while the opened chamber showing the device under test (DUT) is shown on the right hand side.

For the spectral calibration, the device under test is mounted inside the thermal vacuum chamber such that the optical axis of the instrument and the optical axis of the collimator coincide. The chamber is equipped with a germanium window with transmission >90% in the 2 to 14 µm wavelength range.³⁷ During the tests, the chamber was evacuated to $5 \cdot 10^{-7}$ mbar and the blackbody temperature was set to 800°C. The temperature of the DUT was stabilized at 21°C. Bandpass filters with a transmission close to 50% and spectral resolution

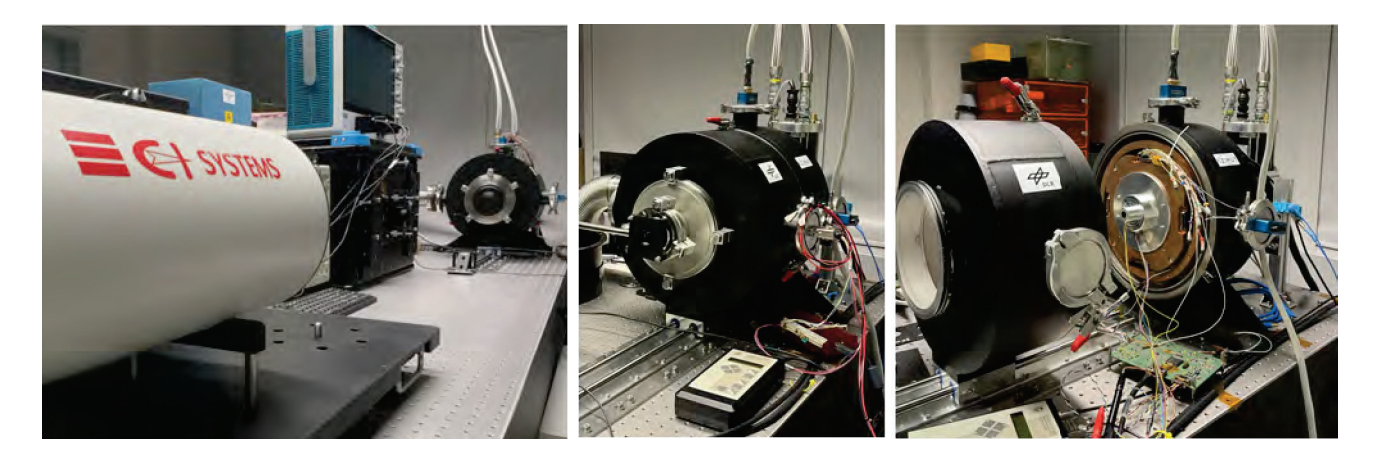


Figure 3: Left: Collimator (foreground) and thermal vacuum cryostat housing the Fabry-Perot spectrometer (background) used for spectral calibration. Middle: Closeup of the thermal vacuum chamber housing the spectrometer with additional bandpass filter mounted in front of the IR-transparent window. Right: Opened chamber showing the device under test mounted to the cryostat's cold plate for temperature stabilization.

 $\lambda/\Delta\lambda$ =50 centered around wavelengths of 7.5, 7.7, 8.0, 8.5, 9.0, 9.035, 9.5, 10.0, 10.35 and 10.5 µm were then successively introduced into the optical path. For each filter, the FPI control voltage was varied between 0 and 70 V and the thermopile response was recorded continuously. For each filter, the maximum thermopile signal, which corresponds to the central wavelength of the bandpass, was then identified.

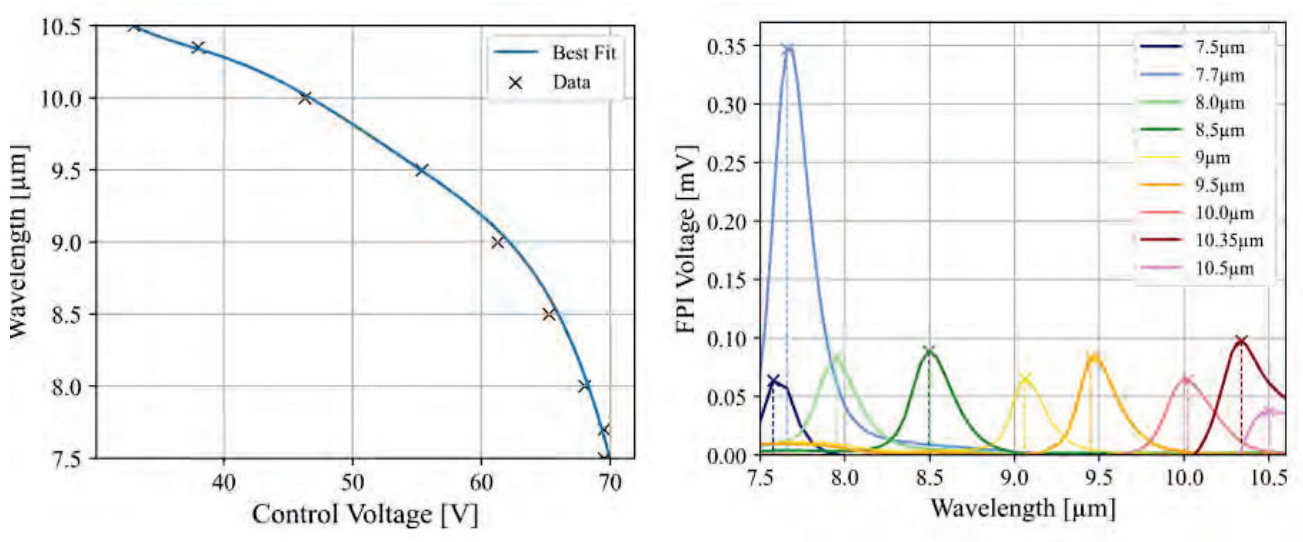


Figure 4: Left: Wavelength corresponding to the maximum signal response as a function of the Fabry-Perot control voltage. Right: Thermopile (FPI spectrometer) signal voltage as a function of wavelength for the 9 bandpass filters employed for spectral calibration. The location of the maximum instrument response for a given filter wavelength is indicated by a cross and associated vertical dashed line.

Results of these measurements are shown on left hand side of Fig. 4, where central filter wavelength is given as a function of thermopile (FPI) voltage along with a 5th order polynomial fit to the data (blue line). This fit serves as the spectral calibration of the instrument and relates control voltage to the wavelength of maximum transmission of the FPI filter. Using this calibration, the data obtained during the measurements can be reformatted to show thermopile (FPI) voltage as a function of wavelength for the different filters (right hand

Filter [µm]	FWHM [µm]	$\lambda/\Delta\lambda$	Hysteresis [µm]	Repeatability [µm]
7.700	0.23	33	0.03	0.14
9.035	0.28	32	0.02	not measured
10.350	0.36	29	0.03	0.02

Table 1: Spectral Resolution $\lambda/\Delta\lambda$ determined from three narrow bandpass filters. The determined Full-Width Half-Maximum of the instrument response and the corresponding measured spectral resolution are given. Further, the hysteresis determined at the different central wavelengths as well as the repeatbility of the measurements are shown.

side of Fig. 4) and the Full-Width Half-Maximum value corresponding to each measurement can be derived. Note that the absolute signal level in the figure is not relevant for the spectral calibration and primarily results from different transmission characteristics of the bandpass filters. Further, it should be noted that this spectral calibration is only valid for measurements taken at the same temperature, as a change in FPI filter temperature leads to shifts in the relationship between center wavelength and control voltage. This is due to the fact that the size of the optical resonator, i.e., the space between the mirror layers, changes as a function of temperature. For the present setup, this temperature dependence was determined to be close to $0.05 \,\mu\text{m/K}$.

Results of the determination of Full-Width Half-Maximum at different central wavelengths are summarized in Tab. 1, where band-passes of 7.7, 9.035, and 10.35 µm have been considered. Full-Width Half-Maximum values of the thermopile response range from 0.23 to 0.36 µm, corresponding to spectral resolutions $\lambda/\Delta\lambda$ around 30. These are thus slightly lower than values previously reported for other filter designs in the visual wavelength range. ^{24–26} In addition to the spectral resolution, hysteresis and repeatability of the design have been investigated for the 7.7 and 10.35 µm band-pass filter. Measurements were carried out by approaching the control voltage corresponding to the central wavelengths from above and below as well as by repeatedly approaching the identical control voltage, respectively. Results of these measurements are also summarized in Tab. 1 and the effects of hysteresis are below 0.03 µm. However, repeatability in the short wavelength range (corresponding to the highest control voltages) can be as large as 0.14 µm. The reason for this behavior is currently unknown and remains to be investigated.

4. SUMMARY AND OUTLOOK

Here we have presented the design of a miniaturized point spectrometer based on thermopile detectors and electrically tunable MEMS Fabry-Perot filters for use under space conditions. The mass of the instrument is estimated to be 105 g for the sensor head and 200 g for the electronics assuming the PCB's will be accommodated inside a central electronics box. The sensor head has a diameter of 40 mm and a length of 45 mm, while the analogue and digital electronics will be housed on a standard PC104-sized PCB each. The current instrument design has been implemented on breadboard level and the current TRL of the sensors including the Fabry-Perot filters is TRL 6. Functional verification of the design has been performed under vacuum conditions and the instrument has been characterized in terms of spectral resolution.

Fabry-Perot transmission was centered around 9 μ m with a usable spectral range between 7.5 and 10.5 μ m. The spectral resolution $\lambda/\Delta\lambda$ achieved with the current design is close to 30, sufficient to resolve broad spectral features like the Christiansen or Transparency Features, which are diagnostic for rock forming minerals. While the hysteresis of the measurements was found to be acceptably small, repeatability of the measurements at high control voltages, corresponding to short wavelengths, remains to be investigated. Further, as a next step in instrument development, the design of the electronics will be completed to assemble a fully functional prototype.

Measurements have been performed under temperature stabilized conditions and it should be noted that the spectral calibration is susceptible to temperature drift. This is due to the temperature dependence of the size of the Fabry-Perot's optical resonator, and the spectral response of the instrument changes at a rate of about $0.05 \, \mu \text{m/K}$. It would therefore be desirable to stabilize the temperature of the sensor head to within $0.1 \, \text{K}$ during

science operations, as was done for radiometers using thermopile detectors on previous missions.^{19,34} If resources on the satellite or lander platform do not allow for a temperature control to be implemented, care must be taken to fully characterize the temperature drift of the spectral calibration during ground testing.

REFERENCES

- [1] Shirley, K. A. and Glotch, T. D., "Particle size effects on mid-infrared spectra of lunar analog minerals in a simulated lunar environment," *Journal of Geophysical Research: Planets* **124**(4), 970–988 (2019).
- [2] Lucey, P. G., Greenhagen, B., Donaldson Hanna, K., Bowles, N., Flom, A., and Paige, D. A., "Christiansen feature map from the lunar reconnaissance orbiter diviner lunar radiometer experiment: Improved corrections and derived mineralogy," *Journal of Geophysical Research: Planets* 126(6), e2020JE006777 (2021).
- [3] Zhang, P., Dai, W., Niu, R., Zhang, G., Liu, G., Liu, X., Bo, Z., Wang, Z., Zheng, H., Liu, C., Yang, H., Bai, Y., Zhang, Y., Yan, D., Zhou, K., and Gao, M., "Overview of the lunar in situ resource utilization techniques for future lunar missions," Space: Science & Eamp; Technology 3, 0037 (2023).
- [4] Lee, S. and van Riessen, A., "A Review on Geopolymer Technology for Lunar Base Construction," *Materials* **15**, 4516 (June 2022).
- [5] Zheng, X., Zhao, C., Sun, X., and Dong, W., "Lunar regolith geopolymer concrete for in-situ construction of lunar bases: A review," *Polymers* 16, 1582 (2024).
- [6] Sargeant, H., Abernethy, F., Barber, S., Wright, I., Anand, M., Sheridan, S., and Morse, A., "Hydrogen reduction of ilmenite: Towards an in situ resource utilization demonstration on the surface of the moon," *Planetary and Space Science* 180, 104751 (2020).
- [7] Sargeant, H. M., Barber, S. J., Anand, M., Abernethy, F. A. J., Sheridan, S., Wright, I. P., and Morse, A. D., "Hydrogen reduction of lunar samples in a static system for a water production demonstration on the Moon," *Plan. Space Sci.* 205, 105287 (Oct. 2021).
- [8] Abdulhamid, F., Sullivan, B. P., and Terzi, S., "Factory in space: A review of material and manufacturing technologies," *Acta Astronautica* **229**, 90–112 (Apr. 2025).
- [9] Silverman, S., Peralta, R., Christensen, P., and Mehall, G., "Miniature thermal emission spectrometer for the mars exploration rover," Acta Astronautica 59(8), 990–999 (2006). Selected Proceedings of the Fifth IAA International Conference on Low Cost Planetary Missions.
- [10] Formisano, V., Angrilli, F., Arnold, G., Atreya, S., Bianchini, G., Biondi, D., Blanco, A., Blecka, M., Coradini, A., Colangeli, L., Ekonomov, A., Esposito, F., Fonti, S., Giuranna, M., Grassi, D., Gnedykh, V., Grigoriev, A., Hansen, G., Hirsh, H., Khatuntsev, I., Kiselev, A., Ignatiev, N., Jurewicz, A., Lellouch, E., Lopez Moreno, J., Marten, A., Mattana, A., Maturilli, A., Mencarelli, E., Michalska, M., Moroz, V., Moshkin, B., Nespoli, F., Nikolsky, Y., Orfei, R., Orleanski, P., Orofino, V., Palomba, E., Patsaev, D., Piccioni, G., Rataj, M., Rodrigo, R., Rodriguez, J., Rossi, M., Saggin, B., Titov, D., and Zasova, L., "The planetary fourier spectrometer (pfs) onboard the european mars express mission," Planetary and Space Science 53(10), 963–974 (2005). First Results of the Planetary Fourier Spectrometer aboard the the Mars Express Mission.
- [11] Gladstone, G. R., Stern, S. A., Retherford, K. D., Black, R. K., Slater, D. C., Davis, M. W., Versteeg, M. H., Persson, K. B., Parker, J. W., Kaufmann, D. E., Egan, A. F., Greathouse, T. K., Feldman, P. D., Hurley, D., Pryor, W. R., and Hendrix, A. R., "LAMP: The Lyman Alpha Mapping Project on NASA's Lunar Reconnaissance Orbiter Mission," Space Science Reviews 150, 161–181 (Jan. 2010).
- [12] Bibring, J.-P., Langevin, Y., Gendrin, A., Gondet, B., Poulet, F., Berthé, M., Soufflot, A., Arvidson, R., Mangold, N., Mustard, J., Drossart, P., and the OMEGA team, "Mars surface diversity as revealed by the omega/mars express observations," *Science* 307(5715), 1576–1581 (2005).
- [13] de Sanctis, M. C., Coradini, A., Ammannito, E., Filacchione, G., Capria, M. T., Fonte, S., Magni, G., Barbis, A., Bini, A., Dami, M., Ficai-Veltroni, I., and Preti, G., "The VIR Spectrometer," space Science Reviews 163, 329–369 (Dec. 2011).
- [14] Peter, G., Helbert, J., Hiesinger, H., Weber, I., Walter, I., Arnold, G., and Säuberlich, T., "Developing of MERTIS as an advanced process from the study up to the flight model," in [Infrared Remote Sensing and Instrumentation XXI], Scholl, M. S. and Páez, G., eds., 8867, 886707, International Society for Optics and Photonics, SPIE (2013).

- [15] Barucci, M. A., Bernardi, P., Reess, J. M., Fornasier, S., Merlin, F., Poggiali, G., David, D., Doressoundiram, A., Gautier, T., Le Du, M., Pieu, V., Sawyer, E., Iwata, T., Nakagawa, H., Nakamura, T., and MIRS Team, , "MIRS: MMX Infrared Spectrometer to Martian System," in [55th Lunar and Planetary Science Conference], LPI Contributions 3040, 1427 (Mar. 2024).
- [16] Paige, D. A., Foote, M. C., Greenhagen, B. T., Schofield, J. T., Calcutt, S., Vasavada, A. R., Preston, D. J., Taylor, F. W., Allen, C. C., Snook, K. J., Jakosky, B. M., Murray, B. C., Soderblom, L. A., Jau, B., Loring, S., Bulharowski, J., Bowles, N. E., Thomas, I. R., Sullivan, M. T., Avis, C., de Jong, E. M., Hartford, W., and McCleese, D. J., "The Lunar Reconnaissance Orbiter Diviner Lunar Radiometer Experiment," Space Science Reviews 150, 125–160 (Jan. 2010).
- [17] Iwata, T., Kitazato, K., Abe, M., Ohtake, M., Arai, T., Arai, T., Hirata, N., Hiroi, T., Honda, C., Imae, N., Komatsu, M., Matsunaga, T., Matsuoka, M., Matsuura, S., Nakamura, T., Nakato, A., Nakauchi, Y., Osawa, T., Senshu, H., Takagi, Y., Tsumura, K., Takato, N., Watanabe, S.-i., Barucci, M. A., Palomba, E., and Ozaki, M., "NIRS3: The Near Infrared Spectrometer on Hayabusa2," Space Science Reviews 208, 317–337 (July 2017).
- [18] Christensen, P. R., Bandfield, J. L., Hamilton, V. E., Ruff, S. W., Kieffer, H. H., Titus, T. N., Malin, M. C., Morris, R. V., Lane, M. D., Clark, R. L., Jakosky, B. M., Mellon, M. T., Pearl, J. C., Conrath, B. J., Smith, M. D., Clancy, R. T., Kuzmin, R. O., Roush, T., Mehall, G. L., Gorelick, N., Bender, K., Murray, K., Dason, S., Greene, E., Silverman, S., and Greenfield, M., "Mars global surveyor thermal emission spectrometer experiment: Investigation description and surface science results," *Journal of Geophysical Research: Planets* 106(E10), 23823–23871 (2001).
- [19] Grott, M., Knollenberg, J., Borgs, B., Hänschke, F., Kessler, E., Helbert, J., Maturilli, A., and Müller, N., "The MASCOT Radiometer MARA for the Hayabusa 2 Mission," *Space Science Reviews* 208, 413–431 (July 2017).
- [20] Bibring, J. P., Hamm, V., Langevin, Y., Pilorget, C., Arondel, A., Bouzit, M., Chaigneau, M., Crane, B., Darié, A., Evesque, C., Hansotte, J., Gardien, V., Gonnod, L., Leclech, J. C., Meslier, L., Redon, T., Tamiatto, C., Tosti, S., and Thoores, N., "The MicrOmega Investigation Onboard Hayabusa2," Space Science Reviews 208, 401–412 (July 2017).
- [21] Wu, Y. and Hapke, B., "Spectroscopic observations of the Moon at the lunar surface," Earth and Planetary Science Letters 484, 145–153 (Feb. 2018).
- [22] Li, X., Gao, M., Liu, J., Li, Y., and Feng, Y., "Design of MWIR hyperspectral imagers based on acousto-optic tunable filters," *Optik* **276**, 170636 (Apr. 2023).
- [23] Valle, S., Ward, J., Pannell, C., and Johnson, N., "Imaging aotfs with low rf power in deep-uv and mid-ir," Physics Procedia 70, 707–711 (2015). Proceedings of the 2015 ICU International Congress on Ultrasonics, Metz, France.
- [24] Rissanen, A., Saari, H., Rainio, K., Stuns, I., Viherkanto, K., Holmlund, C., Näkki, I., and Ojanen, H., "MEMS FPI-based smartphone hyperspectral imager," in [Next-Generation Spectroscopic Technologies IX], Druy, M. A. and Crocombe, R. A., eds., 9855, 985507, International Society for Optics and Photonics, SPIE (2016).
- [25] Tusher, M. M. I., Lee, H., Lee, S., and Lee, K., "Development of a miniaturized pzt-based mems fabry-perot interferometer with eutectic wafer bonding and its interface electronics," *Sensors and Actuators A: Physical* **366**, 114934 (2024).
- [26] Zhou, K., Jing, X., Wang, F., Liu, H., J., H., and W., Z., "Large-aperture electromagnetically actuated mems fabry-perot filtering chips for visible spectral imaging," *Optic express* **31**(22) (2023).
- [27] Kääriäinen T, D. T., "Active hyperspectral imager using a tunable supercontinuum light source based on a MEMS Fabry-Perot interferometer," Opt Lett. 46(22), 5533–5536 (2021).
- [28] Saleh, A., Mekhrengin, M., Dönsberg, T., Kääriäinen, T., Genoud, G., and Toivonen, J., "Mid-infrared hyperspectral sensor based on MEMS Fabry-Pérot interferometer for stand-off sensing applications," *Scientific Reports* 12, 19392 (Nov. 2022).
- [29] Ebermann, M., Neumann, N., Hiller, K., Gittler, E., Meinig, M., and Kurth, S., "Widely tunable Fabry-Perot filter based MWIR and LWIR microspectrometers," in [Next-Generation Spectroscopic Technologies V], Druy, M. A. and Crocombe, R. A., eds., 8374, 83740X, International Society for Optics and Photonics, SPIE (2012).

- [30] Ebermann, M., Neumann, N., Hiller, K., Seifert, M., Meinig, M., and Kurth, S., "Tunable MEMS Fabry-Pérot filters for infrared microspectrometers: a review," in [MOEMS and Miniaturized Systems XV], Piyawattanametha, W. and Park, Y.-H., eds., 9760, 97600H, International Society for Optics and Photonics, SPIE (2016).
- [31] Trops, R., Näsilä, A., Holmlund, C., Toivanen, H., Mannila, R., Stuns, I., Briede, E., Viherkanto, K., Blomberg, M., and Saari, H., "Performance of MOEMS FPI based cubic-inch hyperspectral camera," in [MOEMS and Miniaturized Systems XXI], Zappe, H., Piyawattanametha, W., and Park, Y.-H., eds., 12013, 1201302, International Society for Optics and Photonics, SPIE (2022).
- [32] Neumann, N., Ebermann, M., Kurth, S., and Hiller, K., "Tunable infrared detector with integrated micromachined Fabry-Perot filter," *Journal of Micro/Nanolithography*, MEMS, and MOEMS 7(2), 021004 (2008).
- [33] Meinig, M., Kurth, S., Hiller, K., Neumann, N., Ebermann, M., Gittler, E., and Gessner, T., "Tunable mid-infrared filter based on Fabry-Perot interferometer with two movable reflectors," in [MOEMS and Miniaturized Systems X], Schenk, H. and Piyawattanametha, W., eds., 7930, 79300K, International Society for Optics and Photonics, SPIE (2011).
- [34] Spohn, T., Grott, M., Smrekar, S. E., Knollenberg, J., Hudson, T. L., Krause, C., Müller, N., Jänchen, J., Börner, A., Wippermann, T., Krömer, O., Lichtenheldt, R., Wisniewski, L., Grygorczuk, J., Fittock, M., Rheershemius, S., Spröwitz, T., Kopp, E., Walter, I., Plesa, A. C., Breuer, D., Morgan, P., and Banerdt, W. B., "The Heat Flow and Physical Properties Package (HP³) for the InSight Mission," Space Science Reviews 214, 96 (Aug. 2018).
- [35] Kessler, E. in [Proc. of Sensor 2005, 12th International Conference, Nürnberg], Vol I, 73–78 (2005).
- [36] Mittelholz, A., Stähler, S. C., Kolvenbach, H., Bickel, V., Church, J., Hamran, S. E., Karatekin, O., Ritter, B., Aaron, J., Anhorn, B., Coloma, S., de Palezieux dit Falconnet, L., Grott, M., Ogier, C., Robertsson, J., and Walas, K., "LunarLeaper Unlocking a Subsurface World," in [55th Lunar and Planetary Science Conference], LPI Contributions 3040, 1820 (Mar. 2024).
- [37] Grott, M., Behnke, T., Michaelis, H., Althaus, C., del Togno, S., Wolter, D., Knollenberg, J., and Helbert, J., "A detector characterization setup for testing performance under space environmental conditions," in [Infrared Remote Sensing and Instrumentation XXXI], Strojnik, M. and Helbert, J., eds., 12686, 126860E, International Society for Optics and Photonics, SPIE (2023).
- [38] Grott, M., Wolter, D., Behnke, T., Knollenberg, J., Michaelis, H., Binger, J., Althaus, C., Helbert, J., and Rauer, H., "First results from a detector characterization lab for testing performance under space environmental conditions," in [Infrared Remote Sensing and Instrumentation XXXII], Strojnik, M. and Helbert, J., eds., 13144, 1314403, International Society for Optics and Photonics, SPIE (2024).